CERN – European Organization for Nuclear Research
European Laboratory for Particle Physics

CTF3 Note 025 (Tech.)
(Keyword)

THE RF DEFLECTORS FOR CTF3

D. Alesini, R. Boni, A. Gallo, F. Marcellini

Geneva, Switzerland
18 June 2001

CTFF3 TECHNICAL NOTE

INFN - LNF, Accelerator Division

Frascati, April 18, 2001

Note: **CTFF3-003**

THE RF DEFLECTORS FOR CTF3

D. Alesini, R. Boni, A. Gallo, F. Marcellini

1 Introduction

The bunch train compression scheme for the CLIC Test Facility CTF3 [1] relies on the feasibility of fast RF deflectors.

The most demanding issues in the deflector design are those related to the beam dynamics, including the beam loading effects on the fundamental deflecting mode. On the contrary, the efficiency required by the CTF3 parameters can be easily met by scaling already existing travelling wave (TW) or standing wave (SW) structures.

The injection and the closed bump orbit allowing the multi-turn circulation in the combiner ring require a pair of RF deflectors working at f_{DB}, the Drive Beam (DB) linac frequency, while the injection/extraction in the delay line requires a RF deflector working at $f_{DB}/2$.

Table I: CTF3 RF Deflector Paramenters

	Delay line		Combiner ring	
	TW	SW	TW	SW
nom. Energy E_n [MeV]	184		184	
max. Energy $E_{\max}$ [MeV]	350		350	
frequency f [MHz]	1499.28		2998.55	
number of cells N_c	10	1	10	1
De-phasing/cell	2π/3	---	2π/3	---
total length L [cm]	67	8	33	4
group velocity v_g/c	-.0244	0	-.0244	0
phase velocity v_{ph}/c	1	∞	1	∞
filling time τ_{F_o} [ns]	90	2500	46	900
Shunt impedance $R_s = (E\phi)^2/2P_{RF}$ [MΩ]	0.275	1.2	0.19	0.85
Deflection ϕ [mrad]	10		5	
max RF Power P_{RF} [MW]	22	5.1	8	1.8

The main parameters of the CTF3 RF deflectors are summarized in Table I, comparing the characteristics of traveling wave (TW) and standing wave (SW) structures.

A disk-loaded backward waveguide working in the EH_{11} hybrid mode (RF separator or Langeler structure) [2] already optimized for beam deflection has been considered as a possible TW solution, while a single-cell cavity working in the deflecting TM_{110} mode, obtained by scaling existing designs of crab-crossing cavities, has been taken as a possible SW candidate [3]. In the last case, the shunt impedance values reported in Table I have been specified at the optimal coupling between the SW cavity and the external RF power source. The filling time is $\tau_{F_0} = Q_0/\omega$ in this case. In order to match the pulse length of existing RF source, the filling time τ_F can be shortened by overcoupling the cavity input. In the latter case the effective shunt impedance is decreased by the factor $\left(\tau_F / \tau_{F_0}\right) \cdot \left(2 - \tau_F / \tau_{F_0}\right)$ and the RF power dissipation is increased by the same factor.

Both type of structures meet the CTF3 efficiency requirements, in the sense that they can deliver the required deflection at expense of a reasonable amount of RF power. A TW structure is more promising concerning beam dynamics issues, since wakefields leave the structure faster, due to the shorter filling time, but a rigorous computation of the wake is not trivial.

In the following we report the study of the wake generated by the interaction of the beam with the deflector operating mode (beam loading). Different formulations for the single-passage wake in the TW structure considered in Table I (RF separator) are reported, together with the results of a multi-passage tracking based o the simplest expression of the single-passage wake.

2 Beam loading in RF deflectors

The beam loading in transverse, deflecting structures may be described by two mechanisms:

A. The transverse component of the bunch velocity couples with the deflecting E-field, and the energy exchange creates a deflection gradient along the train;
B. The longitudinal component of the bunch velocity couples with the longitudinal E-field, which is non-zero off axis, and the energy exchange generates an out-of-phase component of the deflecting field.

The first contribution is very similar to the loading of a linac accelerating section or to that of a storage ring RF cavity crossed by a truncated bunch train, and the deflection spread along the train can be estimated obtaining a quite small value in the CTF3 case.

The second contribution is of more concern, because in the combiner ring the bunch pattern is such that at a certain time the deflector will be crossed by bunch trains with a phase separation of only $2\pi/5$ (= 72°), generating a mutual perturbation mainly through the out-of-phase wake. Turn-by-turn the perturbation propagates with the one-turn transport matrix of the ring, and the overall effect may lead to a magnification of the injection errors.

To study this process for a TW structure we worked out a reliable model of the single-passage wake and then we implemented it in a tracking code to analyze the multi-passage effects taking into account the role of the one-turn transport matrix, i.e. of the ring optics.

2.1 Single passage wake

The RF separator fields in cylindrical coordinates (r, ϑ, z) in the region inside the irises $(r \le a)$ at the resonant frequency $\omega^*(v_{ph} = \omega^*/\beta(\omega^*) = c)$ are given by:

$$E_r = jE\frac{k^2a^2 + k^2r^2}{8}\cos(\vartheta) \qquad H_r = jE\frac{k^2a^2 - k^2r^2 - 4}{8Z_0}\sin(\vartheta)$$

$$E_\vartheta = jE\frac{k^2r^2 - k^2a^2}{8}\sin(\vartheta) \qquad H_\vartheta = jE\frac{k^2a^2 + k^2r^2 - 4}{8Z_0}\sin(\vartheta) \qquad (1)$$

$$E_z = \frac{E}{2}kr\cos(\vartheta) \qquad H_z = -\frac{E}{2Z_0}kr\sin(\vartheta)$$

where E is a field scale factor proportional to the square root of the RF power flow in the structure. A charge q crossing the gap in-phase with the deflecting field undergoes a constant Lorentz force $F_\perp = qE/2$. At frequencies $\omega \neq \omega^*$ the field distribution of the mode EH11 becomes much more complicated [4] and may be generically indicated as $\underline{E}^0(\omega)$, $\underline{H}^0(\omega)$.

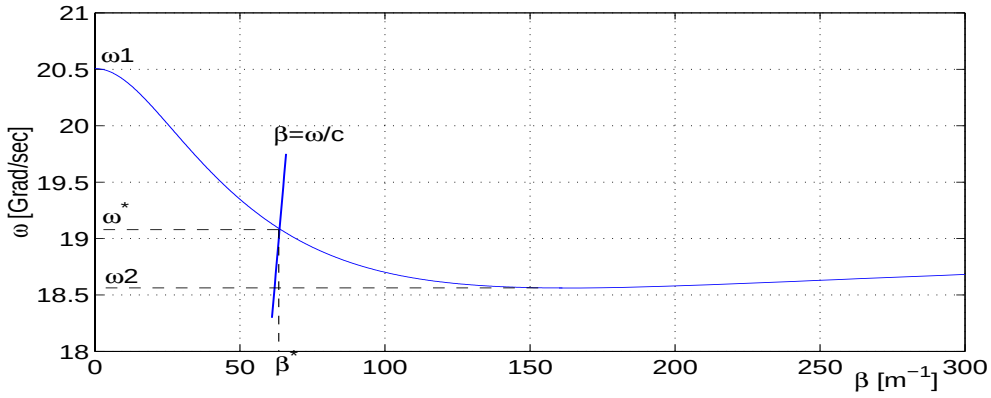

Figure 1: dispersion curve of the RF separator EH_{11} mode

The dependence of the angular frequency ω upon the propagation constant β is shown in the dispersion curve of Fig. 1. The negative group velocity value reported in Tab. I is the derivative of the dispersion curve at ω^*.

Let's consider a charge q crossing the gap along a certain trajectory. The current density $\underline{J}(t)$ and its Fourier transform $\underline{J}(\omega)$ are given by :

$$\underline{J}(t) = q\delta\left(t - \frac{s}{c}\right)\delta(x')\delta(y')\ \underline{s}_0(s)\ ;\ \underline{J}(\omega) = q\, e^{-j\omega s/c}\delta(x')\delta(y')\ \underline{s}_0(s) \qquad (2)$$

where s is the distance along the path, $\underline{s}_0$ is the unit vector tangent to the trajectory, and x',y' are the coordinates on the plane normal to $\underline{s}_0$.

The wave excited by $\underline{J}(t)$ is a superposition of the fundamental EH_{11} mode fields $\underline{E}^0(\omega)$, $\underline{H}^0(\omega)$ weighted by the spectral density coefficient $c^+(\omega,z)$ given by [5];

$$c^+(\omega,z)=\frac{\int_V\left(\underline{E}_\perp^0(\omega)-E_z^0(\omega)\ \underline{z}_0\right)\bullet\underline{J}(\omega)\ e^{j\beta(\omega)z}dV}{2\int_{S_1}\underline{E}_\perp^0(\omega)\times\underline{H}_\perp^0(\omega)\bullet\underline{z}_0dS_1}\approx$$
$$\approx-\frac{q}{4P(\omega)}\int_z^L E_z^0(\omega)\Big|_{\substack{particle\\trajectory}}e^{-j\omega z/c}e^{j\beta(\omega)z'}dz' \qquad (3)$$

where $P(\omega)$ is the flux of the Poynting's vector and the suffix "+" indicates that the wave has a positive phase velocity. Since we are mainly interested in the out-of-phase beam loading, eq. 3 has been obtained assuming that the current density and the EH_{11} mode interact essentially through their longitudinal components.

Back to the time domain, the wave excited by a charge crossing the deflector is given by:

$$\underline{E}^+(t,z)=\frac{1}{\pi}\mathrm{Re}\left[\int_0^{+\infty}c^+(\omega,z)\underline{E}^0(\omega)e^{-j\beta(\omega)z}e^{j\omega t}d\omega\right]$$
$$\underline{H}^+(t,z)=\frac{1}{\pi}\mathrm{Re}\left[\int_0^{+\infty}c^+(\omega,z)\underline{H}^0(\omega)e^{-j\beta(\omega)z}e^{j\omega t}d\omega\right] \qquad (4)$$

The most rigorous evaluation of the single passage wake is obtained by integrating eq. 4 in the pass-band interval (ω_1,ω_2) of the Fig. 1 dispersion curve tacking into account the correct field distribution at each frequency in the band. The transverse wake excited by a leading charge travelling 1 mm off-axis as probed by particles injected out-of-phase with a delay of *T/4* and *T/4* + τ_F*/2* is shown in Fig. 2 (solid lines). The longer is the delay, the more synchronous is the wake and the larger is the Lorentz force on the trailing particle.

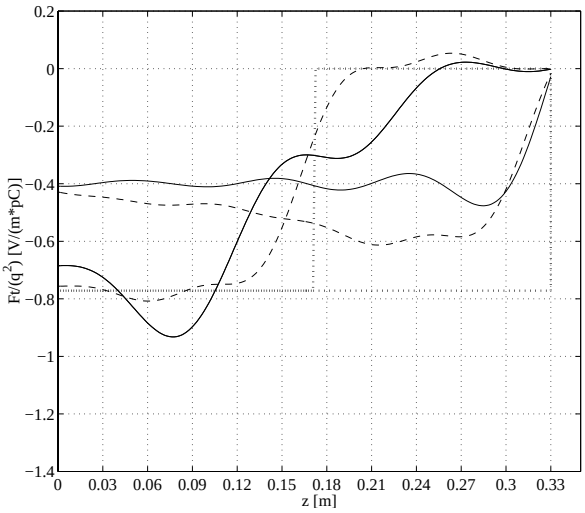

Figure 2: single passage wakes

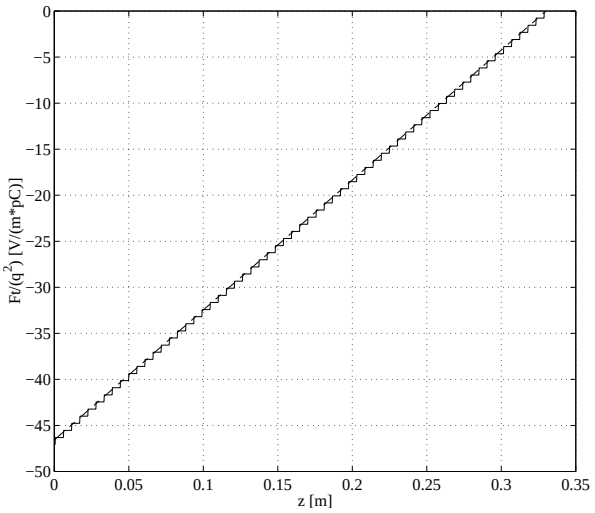

Figure 3: multi-bunch wakes

A significant simplification of the problem is obtained by considering a linear dispersion curve in the pass-band interval and a field distribution equal to the "resonant" one (see eq. 1) for all the frequencies inside the band. The wake computed under this assumption is shown in Fig. 2 (dashed line) and reasonably agrees with the previous one.

A further simplified approach consists in considering only the resonant field configuration of eq. 1 with a local excitation proportional to the leading charge displacement. A rigid wave profile take place, which moves backward with the group velocity. The transverse wake calculated with this method, which is far less accurate and physical with respect to the previous two, is also shown in Fig. 2 (dotted line). It may be demonstrated that this approach is equivalent to the assumption of a linear dispersion curve over an unlimited frequency range. Anyway, in spite of the different qualitative behavior, the amplitude of this last wake is not too different with respect to the other cases.

2.2 Multi-passage tracking

We have considered the effects of the multibunch wake for the bunch pattern of the CTF3 combiner ring. The multibunch wake is obtained by simply adding up the single passage wakes taking into account the bunch pattern. After 1 filling time the multibunch wake converges to a steady state regime solution. It is noticeable that the three different single passage wakes of Fig. 2 produce steady state multibunch wakes that are almost identical, as shown in Fig. 3. The explanation is that the multibunch regime solution is the response to an almost monochromatic excitation, and therefore the details of the dispersion curve out of resonance are not relevant in this case. Therefore the simplest model of single passage wake (corresponding to the dotted line plot of Fig. 2) has been assumed to study the multibunch beam loading in the combiner ring deflectors and, on this base, a simple tracking program has been written to simulate the behavior of the design bunch pattern.

The tracking scheme is sketched in Fig. 4. Each bunch, represented as a macroparticle, enters either deflector with some horizontal initial conditions (x_{in}, x'_{in}), interacts with the main RF deflecting field and with the wake left by the bunches ahead, contributes to the wake and exits the deflector with some new horizontal conditions (x_{out}, x'_{out}). Then the bunch is transported to the other deflector by one of the two transport matrices (M_{12} or M_{21}), interacts with the RF fields before leaving it, and so on up to the extraction.

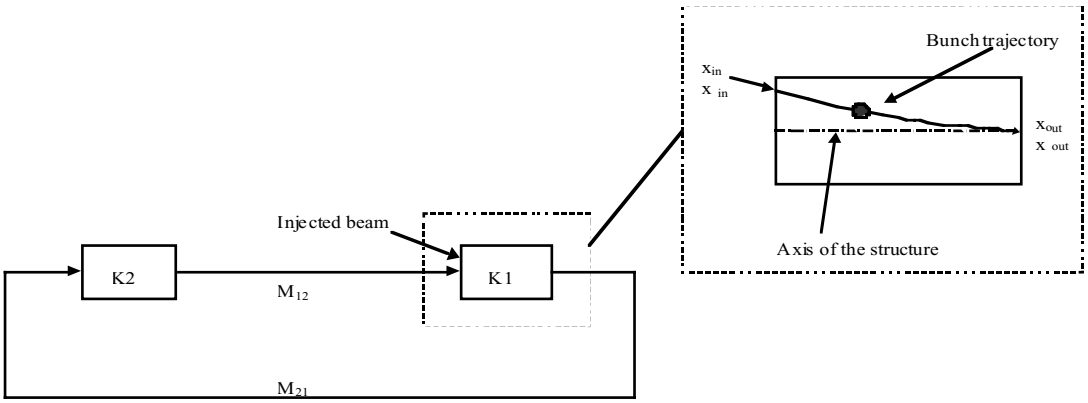

Figure 4: Ring schematics for multi-bunch tracking.

At the end of the merging process each macroparticle ends up with certain horizontal conditions (x_o, x_o') corresponding to a certain value of the Courant-Snyder invariant $I_o = \gamma\, x_o^2 + 2\alpha\, x_o x_o' + \beta\, x_o'^2$ associated with the motion of the bunch center of mass. The tracking is aimed at studying the distribution of the final values of the Courant-Snyder invariant for all bunches, and its dependence on the deflector wakes, the injection errors and the ring tunes.

A) Perfect injection of the 5 trains

We consider first the case of bunch trains injected with the initial conditions that perfectly match the main deflecting field of the deflectors so that, if there were no wake, all the bunches would end up on the combiner design orbit. The 1st train makes the first revolution alone, and there are no bunches interacting with its out-of-phase wake.

During the second revolution, there is the contemporary presence of the 1st and 2nd train, which cross the deflectors with some horizontal displacement. The two trains are interleaved with a separation of 72° RF and their bunches interact through the out-of-phase wake. This generates a first perturbation that deviates the bunches from their ideal trajectories. Similar processes take place during the next interleaving phases, and when the 5 trains are finally merged in a single one, the bunches are spread by a certain extent in the horizontal phase space.

A plot of the position and angle of the bunches with respect to the nominal orbit taken at the 1st kicker output at the end of the merging process is shown in Fig. 5a, while the corresponding plot of the bunch phase space is shown in Fig. 5b. In this case we are considering a 10-cells TW Langeler structure as a RF deflector, and the transport matrices M_{12} and M_{21} are given by the nominal combiner ring optics [6] (Q_x = 7.229). The Fig. 5 plots represent the "systematic effect" since it is not driven by initial injection errors. The average value and the maximum value of the Courant-Snyder invariant distribution of Fig. 5 are respectively $I_{o\_ave} \approx 8 \cdot 10^{-3}$ mm mrad and $I_{o\_\max} \approx 4.2 \cdot 10^{-2}$ mm mrad.

The spread of the macroparticle Courant-Snyder invariant values caused by the systematic effect is therefore a small fraction of the CTF3 bunch design emittance ($\varepsilon \approx 0.5$ mm mrad @ 180 MeV).

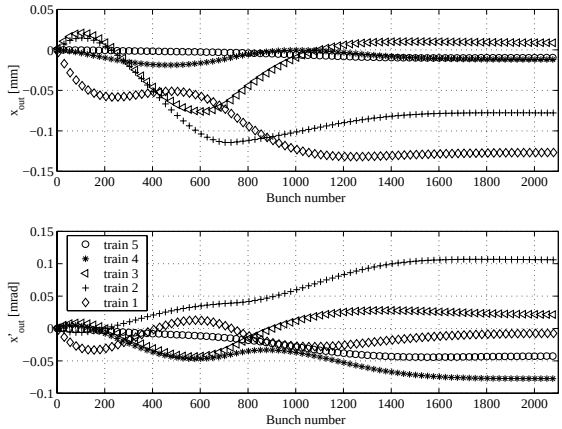

Figure 5a: Position and angle of the bunches of the merged trains

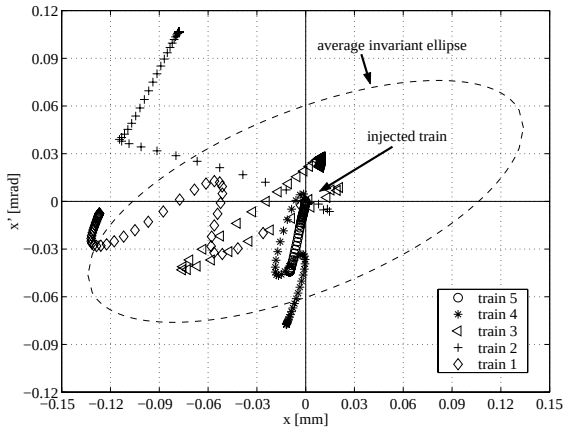

Figure 5b: Phase space footprint of the bunch centers-of -mass of the merged trains

B) Errors in the injection of the trains

The situation is different if the bunches are all injected with a certain position and/or angle error. We considered the case of an error that is equal for all the bunches of a linac pulse, i.e. that is equal for all the 5 incoming trains. This is the case, for instance, if one assumes that the error can fluctuate only from pulse to pulse due to some jitter in the beam transport. The build-up mechanism for the final invariant spread is just the same as previously described, but in this case the initial error can drive the process to larger final errors. The bunch train footprints in the horizontal phase space at the output of the 1st RF deflector for an injection offset of 1 mm and for an injection error of 0.633 mrad in angle (both corresponding to an initial value of the Courant-Snyder invariant $I_{in} \approx$ 0.716 mm mrad) are reported in Fig. 6a and 6b. The statistical properties of the two distributions are summarized in Table II.

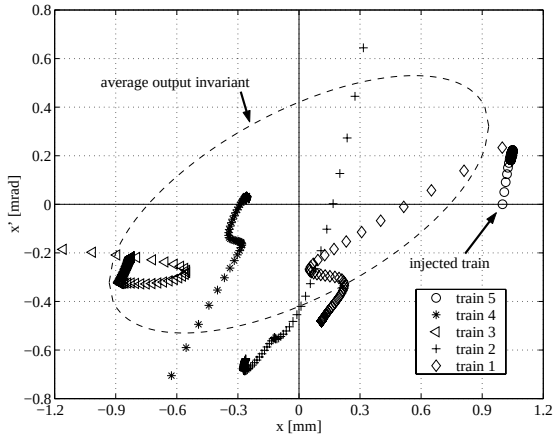

Figure 6a: bunch train phase space footprint for an injection offset of 1 mm

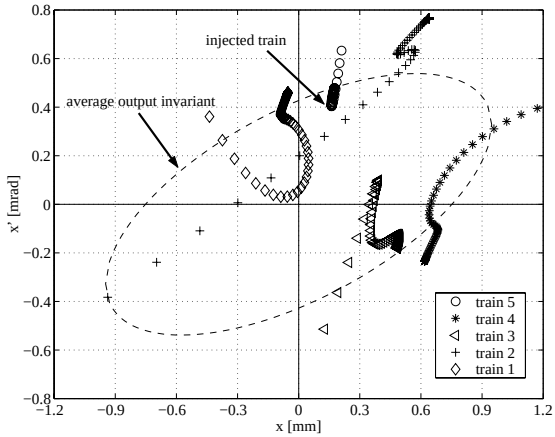

Figure 6b: bunch train phase space footprint for an injection angle of 0.633 mrad

Table II: Statistical properties of the Courant-Snyder invariant of the bunches of the merged trains for an initial value $I_{in} \approx$ 0.716 mm mrad

		x_{in} = 1 mm (see Fig. 6a)	x'_{in} = 0.633 mrad (see Fig. 6b)
Courant-Snyder invariant at the injection	I_{in}	0.716 mm mrad	0.716 mm mrad
Maximum value of the Courant-Snyder invariant at the extraction	$I_{o\_\max}$	0.814 mm mrad	0.850 mm mrad
Average value of the Courant-Snyder invariant at the extraction	I_{o_ave}	0.392 mm mrad	0.405 mm mrad
Standard deviation of the Courant-Snyder invariant at the extraction	σ_{I_o}	0.231 mm mrad	0.203 mm mrad

We may conclude that, in general, the maximum value $I_{o\_\max}$, the average value I_{o_ave} and the standard deviation σ_{I_o} of the final distributions are not constant for a given I_{in}, but, due to the nature of the wake, depend also on the betatron phase of the bunch train at the injection. If we consider all the possible betatron phases for a given I_{in}, and calculate the maximum and average values for the corresponding final distributions, we obtain the 3D plots of Fig. 7. For any given initial I_{in} value, there are some betatron phases giving the largest $I_{o\_\max}$ value ($\hat{I}_{o\_\max}$), and the largest I_{o_ave} value ($\hat{I}_{o\_ave}$).

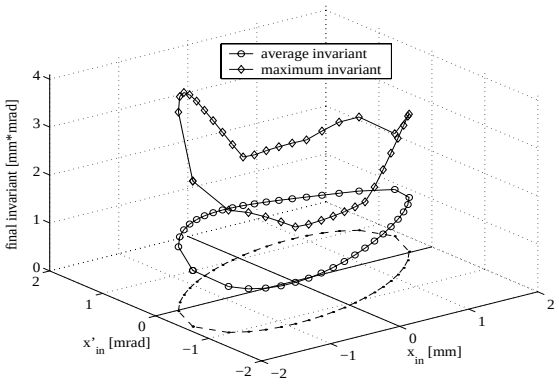

Figure 7: $I_{o\_\max}$ and I_{o_ave} for a given I_{in} for various betatron phases

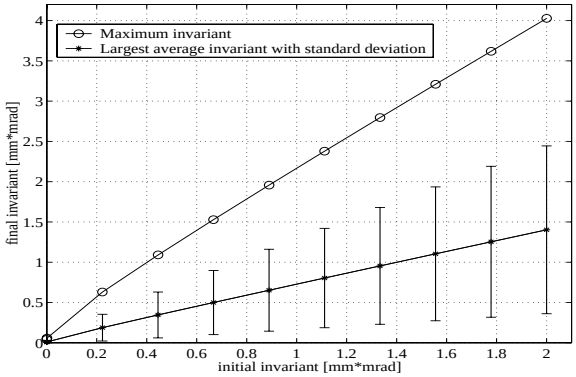

Figure 8: $\hat{I}_{o\_\max}$ and $\hat{I}_{o\_ave}$ as function of the injection Courant-Snyder invariant

The plots of $\hat{I}_{o\_\max}$ and $\hat{I}_{o\_ave}$ (this last including the ± 1 standard deviation bar) for I_{in} ranging from 0 to 2 mm mrad are shown in Fig. 8. It may be seen that, assuming the nominal optics parameters, it is always $\hat{I}_{o\_ave} < I_{in}$, which means that, on the average, the deflectors wake gives a sort of "cooling" of the Courant-Snyder invariant of the bunch center-of-mass. On the other hand from Fig. 8 one has $\hat{I}_{o\_\max} / I_{in} \le 2.6$, which means that, in the worst case and for the worst bunch, the magnification of the injection error is a factor $\le \sqrt{2.6} \approx 1.6$. The magnification factor is reduced to $\le \sqrt{1.5} = 1.23$ for all bunches staying within +1 standard deviation above the average (≈ 70% of the bunches).

The minimization of these magnification factors is one of the criteria for the choice of the ring horizontal tune. Different tunes may result in very different magnification factors. For example, we report in Fig. 9 the ratio I_{o_ave} / I_{in} and $I_{o\_\max} / I_{in}$ in the case of an injection error caused by a pure displacement of 1 mm for various values of the betatron phase advance in the M_{21} matrix. Our nominal tune corresponds to a phase advance of 262°, which is close to the minimum. Modifications of the phase advance in the range of ±10° (corresponding to variations of the tune value of ≈ ± .03) does not significantly change the scenario. Anyway, some tunes outside the range shown in Fig. 9 may give magnification factors larger than 10 [7].

Studies of the beam loading effects based on tracking simulations will continue to investigate other aspects. The most important items to be analyzed are:

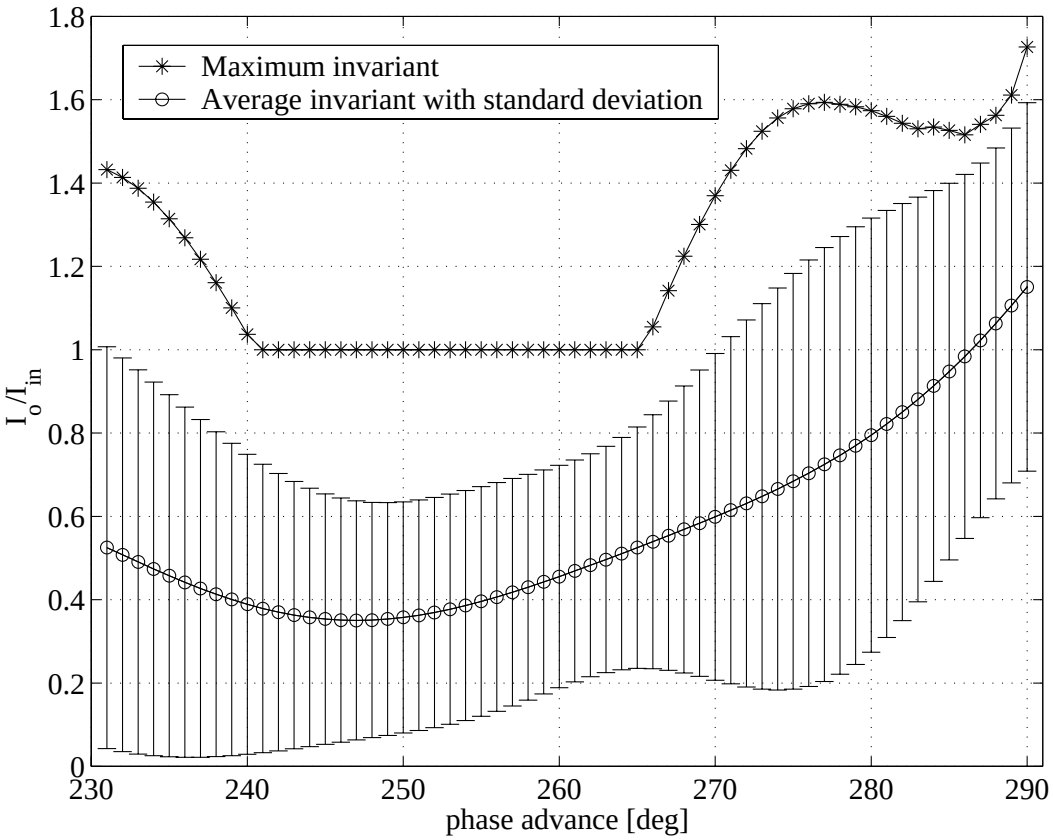

Figure 9: Tune dependence of the Courant-Snyder invariant magnification for an injection offset of 1 mm

A) Contribution of the RF structure modes different from the operational one to the final quality of the merged train. In particular, the vertical polarity of the operational mode, which is detuned by some asymmetry in the cells, has to be anyway taken into account, since the vertical tune of the ring may be far from optimum.

B) Different injection conditions for "odd" and "even" bunches in each incoming train due to the "memory" of the different paths in the delay loop.

C) Beam loading effects due to off-time injection and finite bunch length.

3 The delay loop RF deflector

The dynamics implications of the RF deflector for the delay loop are less demanding, and this is mainly due to the bunch pattern in the deflector since there are no bunches probing the out-of-phase wake in this case.

The operating frequency of this device will be 1.5 GHz and there are not RF power sources re-usable to excite the required deflecting field. This adds one more degree of freedom in designing the structure, since there are a certain number of options in the market concerning the power level of the source and the pulse duration.

An obvious possibility is that of scaling a Langeler structure to 1.5 GHz. In this case the expected behavior for the beam dynamics is excellent, but the size of the structure is quite large. Since the beam loading requirement are relaxed for the delay loop deflector with respect to the combiner ring ones, we can in principle consider other options in this case, such as standing wave cavities that are more compact and efficient (see Tab. I). A longer RF pulse could be required in this case to fill the cavity at its best efficiency. The filling time can be shortened by properly over-coupling the cavity input, at the expense of the reduction of the efficiency. A possible standing wave RF deflector could be designed starting from already proposed geometry for crab-cross cavities or standing wave separators. An HFSS model of a single cell, standing wave deflecting cavity is shown in Fig. 10.

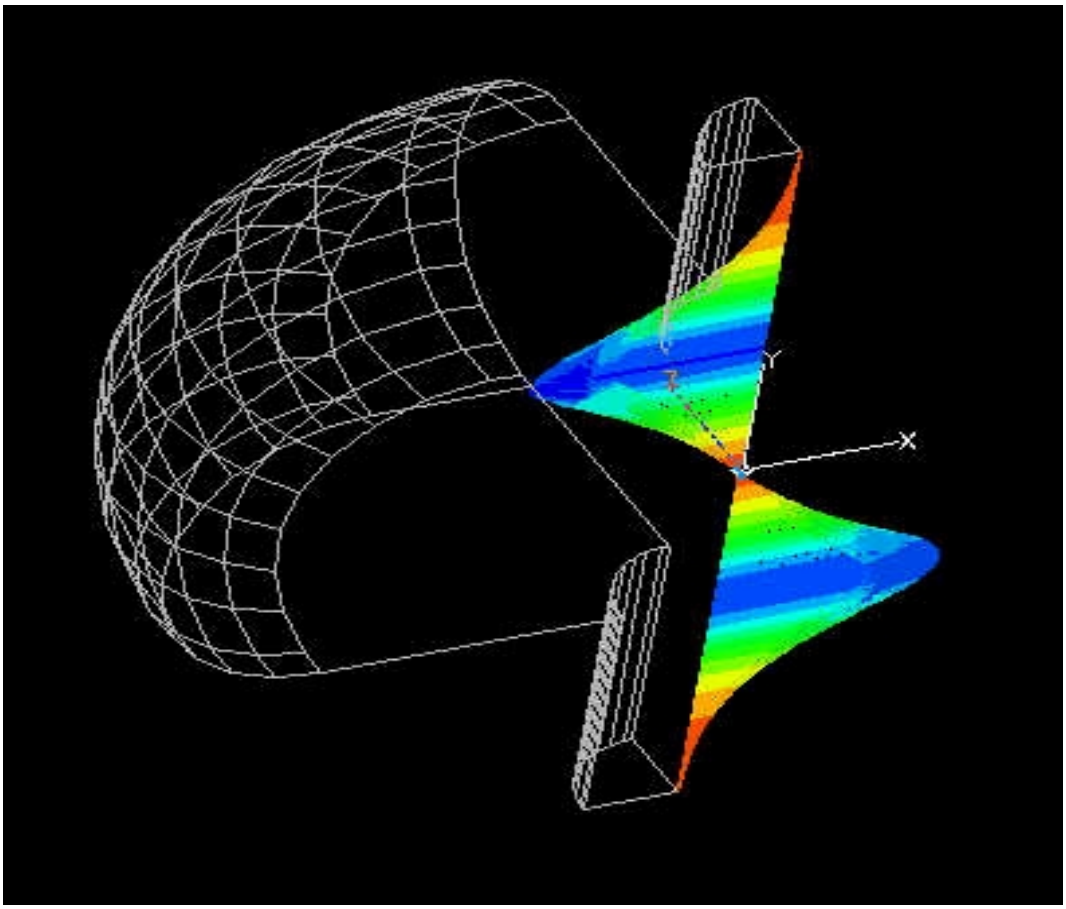

Figure 10: HFSS model of a SW single-cell cavity

4 RF deflector design activities

The simulation results reported in the previous section indicate that a proper choice of the combiner ring horizontal tune keeps under control the beam loading effects of a pair of Langler structures. For that reason a design activity aimed at constructing two RF deflectors of this type in less than one-year time has been started. Mechanical drawings of such a RF structure scaled at 3 GHz frequency have been almost completed and a sketch is reported in Fig. 11, while only some details, like the geometry of the of the two terminal cells, are still under study.

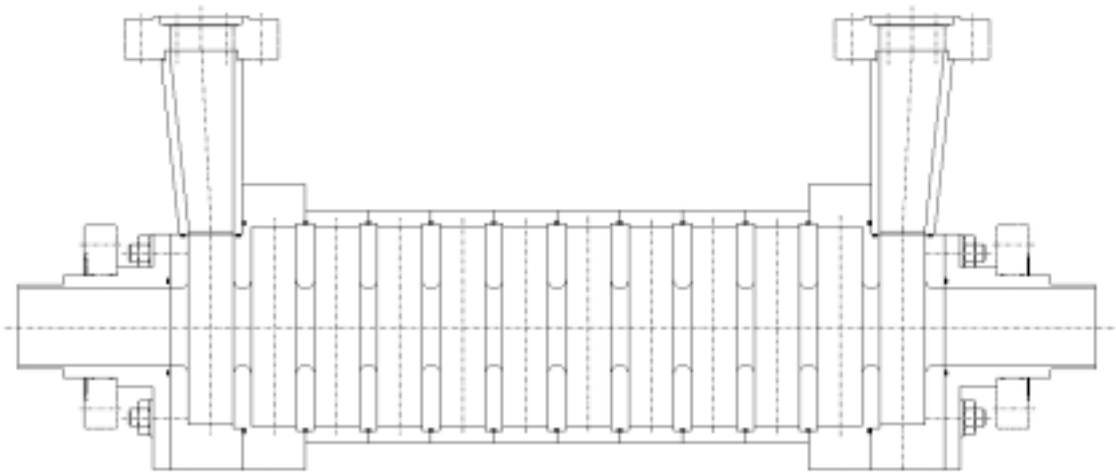

Figure 11: Mechanical sketch of a 3 GHz, 10 cells Langeler structure

The study of the structure is mainly addressed by the fundamental papers and it is based on 3D simulations that make use of the well known MAFIA and HFSS codes. Although the codes are very powerful, some aspects of the design need to be experimentally confirmed. For that reason the construction of an aluminum prototype suitable for laboratory measurements and flexible enough to allow the experimental characterization of different options has been decided.

Acknowledgements

The authors would like to thank M. Preger and M. Zobov for their help in reviewing the manuscript, and P. Possanza for the final editing.

References

[1] H.H. Braun et al., CERN 99-06, 1999.
[2] P. Bernard et al., CERN 68-30, 1968.
[3] K. Akai et al., SLAC-0400,1992, p.181.
[4] Y. Garault, CERN 64-43, 1964.
[5] R.E. Collin, "Foundation for microwave engineering", Mc Grow-Hill, 1992.
[6] C. Biscari et al., Proc. of the EPAC 2000 conf., p. 450.
[7] A. Gallo et al., Proc. of the EPAC 2000 conf., p. 465.